EPJ Web of Conferences **3**, 06008 (2010)
DOI:10.1051/epjconf/20100306008

Neutron-Proton Mass Difference in Nuclear Matter and in Finite Nuclei and the Nolen-Schiffer Anomaly

U.-G. Meißner[1,2,3], A.M. Rakhimov[4,5], A. Wirzba[2,3,a], and U.T. Yakhshiev[2,6]

[1] Helmholtz-Institut für Strahlen- und Kernphysik and Bethe Center for Theoretical Physics, Universität Bonn, D-53115 Bonn, Germany
[2] Institut für Kernphysik and Jülich Center for Hadron Physics, Forschungszentrum Jülich, D-52425 Jülich, Germany
[3] Institute for Advanced Simulation, Forschungszentrum Jülich, D-52425 Jülich, Germany
[4] Institute of Nuclear Physics, Academy of Sciences of Uzbekistan, Tashkent-132, Uzbekistan
[5] Institute of Physics and Applied Physics, Yonsei University, Seoul, 120-749, Korea
[6] Physics Department and Institute of Applied Physics, National University of Uzbekistan, Tashkent-174, Uzbekistan

Abstract. The neutron-proton mass difference in (isospin asymmetric) nuclear matter and finite nuclei is studied in the framework of a medium-modified Skyrme model. The proposed effective Lagrangian incorporates both the medium influence of the surrounding nuclear environment on the single nucleon properties and an explicit isospin-breaking effect in the mesonic sector. Energy-dependent charged and neutral pion optical potentials in the s- and p-wave channels are included as well. The present approach predicts that the neutron-proton mass difference is mainly dictated by its strong part and that it markedly decreases in neutron matter. Furthermore, the possible interplay between the effective nucleon mass in finite nuclei and the Nolen-Schiffer anomaly is discussed. In particular, we find that a correct description of the properties of mirror nuclei leads to a stringent restriction of possible modifications of the nucleon's effective mass in nuclei.

1 Introduction

This presentation is about a calculation of the neutron-proton mass difference in finite nuclei and in nuclear matter in the framework of a medium-modified Skyrme model.

The nuclear-density dependence of isospin-breaking effects belongs to one of the fundamental questions in nuclear physics [1–3]. In particular, the effective neutron-proton mass difference in finite nuclei and nuclear matter $\Delta m^*_{\rm np}$, although it is of astrophysical relevance, of importance for the description of mirror nuclei, the stability of drip-line nuclei etc., is not very well under control. Rather, there exist very different theoretical predictions of this quantity for isospin-asymmetric nuclear mater [4–17] which predict both qualitatively and quantitatively different results.

Most notably, the in-medium neutron-proton mass difference is relevant for the description of mirror nuclei and the Nolen-Schiffer anomaly (NSA) [18, 19]. Although there are many theoretical approaches devoted to the explanation of the NSA discrepancy [20–31] this phenomenon is still not fully understood.

Skyrme-soliton models have the inherent advantage, compared with other hadronic models, that they are based on chiral input (chiral Lagrangians in the meson sector) and that they treat the *structure*, *properties* and *interactions* of the investigated nucleons on an equal footing [32–37]. Moreover, Skyrme-soliton models allows for an easy incorporation of the nuclear background via local medium-dependent coefficients [38–40]. They are therefore well suited to address the problem of the medium-dependence of the effective neutron-proton mass splitting and the Nolen-Schiffer anomaly. In Refs. [42, 43] we investigated $\Delta m^*_{\rm np}$ in symmetric and asymmetric nuclear matter, respectively. Here we rather focus on the results of Ref. [44] which addresses the behavior of this quantity in finite nuclei and the Nolen-Schiffer anomaly.

The presentation is organized as follows. In Sect. 2 we review how the Skyrme model should be generalized in order to include explicit isospin breaking and explicit chiral breaking on the same footing. An unconventional breaking mechanism is introduced and the relevant quantization procedure is discussed. Section 3 is dedicated to the introduction of medium-modifications to the isospin-extended Skyrme model. We review the construction of the medium-modified Skyrme model based on the pion dispersion in a nuclear background. Section 4 focusses on the static results of the nucleon when the pertinent skyrmion is placed at the center of spherical symmetric nuclear core. The construction of the electromagnetic part of the in-medium neutron-proton mass splitting is indicated. Values for the effective proton mass, the (total and electromagnetic contribution of the) in-medium neutron-proton mass splitting, the proton and neutron magnetic moments and the scalar and isovector rms-radii are reported. In Sect. 5 we discuss the in-medium neutron-proton mass difference when the nucleon is located at a distance R from the center. Corresponding

[a] e-mail: a.wirzba@fz-juelich.de

results in infinite nuclear matter can be found in Sect. 6. In Sect. 7 tentative conclusions are given to the behavior of the effective shift $\Delta m^*_{\rm np}$. The Nolen-Schiffer anomaly and the prediction of the medium-modified generalized Skyrme model are discussed in Sect. 8. We end the presentation with final remarks in Sect. 9.

2 Isospin-modified Skyrme model

2.1 Generalized symmetry breaking

The standard Skyrme model [32–37] consists of the non-linear σ-model Lagrangian, which is of second order in the derivatives, and a fourth order soliton-stabilizing term:

$$\mathcal{L} = \frac{F_\pi^2}{16}\mathrm{Tr}\left(\partial_\mu U \partial^\mu U^\dagger\right) + \frac{1}{32e^2}\mathrm{Tr}[U^\dagger\partial_\mu U, U^\dagger\partial_\nu U]^2, \quad (1)$$

where

$$U(x) = \exp\left(2\mathrm{i}\sum_{a=1}^{3}\tau^a\pi^a(x)/F_\pi\right) = 1 + \mathrm{i}\frac{2\tau\cdot\pi}{F_\pi} + \cdots \quad (2)$$

is the usual chiral SU(2) matrix formulated in terms of the pion field π^a. The pion-decay constant F_π (its physical value would have been 186 MeV) and the stabilizing parameter e are normally – and also here – adjusted in such a way, that, after rigid-rotator quantization in the (baryon number) B=1 soliton sector, the empirical isospin-averaged nucleon and delta masses are fitted. Note that the usual Skyrme model preserves isospin symmetry. This holds even if there is a chiral symmetry breaking term

$$\mathcal{L}_{\rm SB} = \frac{F_\pi^2 m_\pi^2}{16}\mathrm{Tr}\left(U + U^\dagger - 2\right) \quad (3)$$

present, which induces the pion-mass term in the (B=0) meson-sector of the model, see especially [33, 35–37]. In order to incorporate explicit chiral symmetry breaking and isospin-breaking on equal footing as it is the case for the free pion Lagrangian

$$\mathcal{L}_{\rm mes} = \partial_\mu\pi^+\partial^\mu\pi^- - m^2_{\pi^\pm}\pi^+\pi^- + \tfrac{1}{2}\left(\partial_\mu\pi^0\partial^\mu\pi^0 - m^2_{\pi^0}\pi^0\pi^0\right),$$
$$\pi^\pm = \tfrac{1}{\sqrt{2}}(\pi_1 \mp i\pi_2), \quad \pi^0 = \pi_3,$$

the original Skyrme model has to be modified. Following Rathske [41] we therefore add to the ordinary Skyrme Lagrangian (1) the following generalized symmetry breaking term

$$\mathcal{L}_{\rm g\chi SB} = -\frac{F_\pi^2}{16}\Big\{\mathrm{Tr}\left[(U-1)\overline{\mathcal{M}}^2(U^\dagger-1)\right] - \mathrm{Tr}\left[(U-1)\tau_3\mathcal{M}_\Delta^2(U^\dagger-1)\tau_3\right]\Big\}, \quad (4)$$

which explicitly breaks chiral symmetry and isospin symmetry. Here the following definitions have been applied:

$$\overline{\mathcal{M}}^2 \equiv \tfrac{1}{2}(m^2_{\pi^\pm} + m^2_{\pi^0}), \quad \mathcal{M}_\Delta^2 \equiv \tfrac{1}{2}(m^2_{\pi^\pm} - m^2_{\pi^0}) \quad (5)$$

with $m_{\pi^\pm} \equiv m^{\rm strong}_{\pi^\pm}$ denoting the strong-interaction part of the mass of the charged pions. Note that the electromagnetic contribution to the latter mass is beyond the framework of the present model and will not be considered here.

2.2 Quantization

Following Refs. [42–44], we quantized the isospin-modified Skyrme model with the help of one constrained (φ_3^c(t)) and three unconstrained time-dependent collective coordinates ($\varphi_1(t), \varphi_2(t), \varphi_3(t)$)

$$U \to AUA^\dagger \quad \text{with} \quad A \to A(t) = \exp\left(\mathrm{i}\,\tau\cdot\varphi/2\right) \quad (6)$$

where

$$\dot\varphi_1 = \omega_1, \quad \dot\varphi_2 = \omega_2, \quad \dot\varphi_3 = \omega_3 + \dot\varphi_3^c \equiv \omega_3 + a_c \quad (7)$$

are the pertinent angular velocities. Under the spherical hedgehog ansatz $U(\mathbf{r}) = \exp(\mathrm{i}\tau\cdot\hat{\mathbf{r}}F(r))$, there exist also collective coordinates linked to static rotations of the skyrmion in coordinate space, where $\Omega_1, \Omega_2, \Omega_3$ are the relevant angular velocities. In terms of both classes of angular velocities the spatially integrated Skyrme Lagrangian (1) including the generalized symmetry breaking term (4) turns into

$$L \equiv \int \mathrm{d}^3r\left\{\mathcal{L}_2 + \mathcal{L}_4 + \mathcal{L}_{\rm g\chi SB}\right\} = -M_{\rm NP} - \mathcal{M}_\Delta\Lambda_2 + \tfrac{1}{2}(\overbrace{\Lambda_2 + \Lambda_4}^{\Lambda})\left[(\omega_1-\Omega_1)^2 + (\omega_2-\Omega)^2 + (\omega_3-\Omega_3+a_c)^2\right]$$
$$= -M_{\rm NP} + \tfrac{1}{2}\Lambda\sum_{i=1}^3(\omega_i-\Omega_i)^2 + \Lambda(\omega_3-\Omega_3)a_c, \quad (8)$$

where $M_{\rm NP}$ is the static soliton mass when it is non-perturbed (NP) by isospin-breaking. It is the hedgehog mass in case the above-mentioned hedgehog ansatz is inserted for the time-independent chiral matrix. Λ_2 and Λ_4 are the moments of inertia of the non-linear σ model Lagrangian $\mathcal{L}_2$ and the fourth-order stabilizing term $\mathcal{L}_4$, respectively. In the last line of Eq. (8), we employed the constraint

$$\mathcal{M}_\Delta\Lambda_2 = \tfrac{1}{2}\Lambda a_c^2, \quad (9)$$

whose role is to balance the isospin-breaking terms, such that the hedgehog ansatz of the usual Skyrme model can still be applied. In terms of the canonical conjugate momentum operators $\hat T_i \equiv \partial L/\partial\omega_i$ (and $\hat J_i \equiv \partial L/\partial\Omega_i = -\hat T_i$) corresponding to isospin (and spin), the pertinent Hamiltonian becomes

$$H = M_{\rm NP} + \tfrac{1}{2}\Lambda a_c^2 + \frac{\hat{\mathbf{T}}^2}{2\Lambda} - a_c\hat T_3,$$

while the baryon states are $|T, T_3, J = T, J_3 = -T_3\rangle$. When the Hamiltonian is sandwiched by these states, the energy of a nucleon of isospin component $\pm\frac{1}{2}$ is determined as

$$m_{\rm p/n} \equiv E_{\rm p/n} = M_{\rm NP} + \tfrac{1}{2}\Lambda a_c^2 + \tfrac{3}{8\Lambda} \mp a_c\tfrac{1}{2}. \quad (10)$$

The latter equation allows to isolate the strong part of the neutron-proton mass difference as $\Delta m^{\rm strong}_{\rm np} = a_c$ with

$$a_c = \sqrt{\frac{2\mathcal{M}_\Delta}{\Lambda}} \approx (1.291 + 0.686)\,\mathrm{MeV}. \quad (11)$$

For consistency, the empirical electromagnetic contribution −0.686 MeV to the in-vacuum value 1.291 MeV of the neutron-proton mass difference had to be subtracted.

3 Medium-modifications

The explicit isospin-breaking term is only one part contributing to the neutron-proton mass difference in a nucleus or nuclear matter. The other part comes from the isospin asymmetry of the nuclear background. In order to include this asymmetry into the nuclear-background parameters of a medium-modified Skyrme model, used in Refs. [38–40], we start out by introducing medium-modifications to the free pion Lagrangian (4).

Note that throughout this presentation we will denote medium-modified Langrange terms, energies, masses, moments of inertia, form factors, etc. with an explicit asterix.

3.1 Pion dispersion in a nuclear background

The pertinent medium-modified Lagrangian of the pion field can be formulated in terms of the self-energies (*i.e.* energy-dependent optical potentials) of the charged pions as follows:

$$\mathcal{L}^*_{\rm mes} = \sum_{\lambda=\pm,0}\left\{\tfrac{1}{2}\partial_\mu\pi^{\lambda\dagger}\partial^\mu\pi^\lambda - \tfrac{1}{2}\pi^{\lambda\dagger}\Big(m^2_{\pi^\lambda} + \hat{\Pi}^\lambda(\omega,\mathbf{r})\Big)\pi^\lambda\right\}$$
$$= \mathcal{L}_{\rm mes} - \tfrac{1}{2}\left\{\pi_a\tfrac{\hat{\Pi}^- + \hat{\Pi}^+}{2}\pi_a + \mathrm{i}\,\varepsilon_{ab3}\,\pi_a\,\tfrac{\hat{\Pi}^- - \hat{\Pi}^+}{2}\,\pi_b\right\}. \quad (12)$$

In the local density approximation the s-wave self-energies become

$$\hat{\Pi}^\pm_s(\omega,\mathbf{r}) = -4\pi\Big(b_0^{\rm eff}(\omega)\,\rho(\mathbf{r}) \mp b_1(\omega)\delta\rho(\mathbf{r})\Big)\eta \quad (13)$$

with the total and isosvector density

$$\rho(\mathbf{r}) = \rho_n(\mathbf{r}) + \rho_p(\mathbf{r}), \quad \delta\rho(\mathbf{r}) = \rho_n(\mathbf{r}) - \rho_p(\mathbf{r}) \quad (14)$$

and $\eta \equiv 1 + m_\pi/m_N$ in terms of the isospin-averaged pion and nucleon masses. The effective isoscalar and isovector pion-nucleon scattering lengths can be expressed as

$$b_0^{\rm eff}(\omega) \approx b_0(\omega) - \frac{3k_F}{2\pi}\Big[b_0^2(\omega) + 2b_1^2(\omega)\Big], \quad (15)$$

$$b_0(\omega) \approx -\tilde{b}_0\Big(1 - m_\pi^{-2}\omega^2\Big)/(4\pi\eta), \quad (16)$$

$$b_1(\omega) \approx \tilde{b}_1\Big(m_\pi^{-1}\omega + 0.143 m_\pi^{-3}\omega^3\Big)/(4\pi\eta) \quad (17)$$

in terms of the total Fermi momentum k_F and the parameters $\tilde{b}_0 = -1.206\,m_\pi^{-1}$, $\tilde{b}_1 = -1.115\,m_\pi^{-1}$. The corresponding p-wave self-energies read in the local density approximation

$$\hat{\Pi}^\pm_p(\omega,\mathbf{r}) = \nabla\frac{4\pi c^\pm(\omega,\mathbf{r})}{1 + 4\pi g' c^\pm(\omega,\mathbf{r})}\cdot\nabla$$
$$- \frac{4\pi\omega}{2m_N}\Big(\nabla^2 c^\pm(\omega,\mathbf{r})\Big) \quad (18)$$

with $g' = 0.47$ and

$$c^\pm(\omega,\mathbf{r}) \equiv \Big(c_0(\omega)\,\rho(\mathbf{r}) \mp c_1(\omega)\,\delta\rho(\mathbf{r})\Big)/\eta \quad (19)$$

in terms of the isoscalar and isovector pion-nucleon scattering volumes $c_0 = 0.21 m_\pi^{-3}$ and $c_1 = 0.165\,m_\pi^{-3}$, respectively; see Refs. [43,44] for more details on the parameters and references.

3.2 Medium-modified generalized Skyrme model

Marrying the generalized isospin-modified Skyrme model of Rathske [41] with the in-medium modified Skyrme model of Refs. [38–40] (which is characterized by density dependent coefficients of the second order symmetry-conserving and breaking Lagrangian terms) and extending it to asymmetric nuclear background as in Eq. (12), one arrives at the following isospin- and medium-modified Skyrme Lagrangian [42–44]:

$$\mathcal{L}^* = \mathcal{L}_2^* + \mathcal{L}_4 + \mathcal{L}^*_{\chi\rm SB} + \Delta\mathcal{L}_{\rm mes} + \Delta\mathcal{L}^*_{\rm env}, \quad (20)$$

$$\mathcal{L}_2^* = \frac{F_\pi^2}{16}\Big\{\Big(1 + \frac{\chi_s^{02}}{m_\pi^2}\Big)\mathrm{Tr}\left(\partial_0 U\partial_0 U^\dagger\right)$$
$$- \left(1 - \chi_p^0\right)\mathrm{Tr}(\nabla U\cdot\nabla U^\dagger)\Big\},$$

$$\mathcal{L}_4 = \frac{1}{32e^2}\,\mathrm{Tr}\,[U^\dagger\partial_\mu U, U^\dagger\partial_\nu U]^2,$$

$$\mathcal{L}^*_{\chi\rm SB} = -\frac{F_\pi^2 m_\pi^2}{16}\Big(1 + m_\pi^{-2}\chi_s^{00}\Big)\,\mathrm{Tr}\Big[(U-1)(U^\dagger - 1)\Big],$$

$$\Delta\mathcal{L}_{\rm mes} = -\frac{F_\pi^2}{16}\sum_{a=1}^{2}\frac{m^2_{\pi^\pm} - m^2_{\pi^0}}{2}\,\mathrm{Tr}(\tau_a U)\mathrm{Tr}(\tau_a U^\dagger),$$

$$\Delta\mathcal{L}^*_{\rm env} = -\frac{F_\pi^2}{16}\sum_{a,b=1}^{2}\varepsilon_{ab3}\frac{\Delta\chi_s + \Delta\chi_p}{2m_\pi}\,\mathrm{Tr}(\tau_a U)\mathrm{Tr}(\tau_b\partial_0 U^\dagger).$$

Here $\mathcal{L}_{\rm mes}$ is the *explicitly* isospin-breaking Lagrangian, while $\Delta\mathcal{L}^*_{\rm env}$ summarizes the *enviroment-induced* isospin-breaking contribution. The second-order Lagrangians $\mathcal{L}_2^*$ and $\mathcal{L}_{\chi\rm SB^*}$ are isospin-symmetric, but explicitly medium-dependent, whereas $\mathcal{L}_4$ is neither isospin-breaking nor medium-dependent. We preserve the original term for stabilizing skyrmions and do not modify it by, *e.g.* higher-order derivative terms or vector-meson contributions, since it is on the one hand generic for our purposes and on the other hand still simple to handle.

The medium functionals appearing in $\mathcal{L}_2^*$ and $\mathcal{L}^*_{\chi\rm SB}$ are constructed by the rule $\hat{\Pi}(\omega) \to \hat{\Pi}(i\partial_0)$ from the input of Sect. 3.1 and take the form:

$$\chi_s^{00} = \left(\tilde{b}_0 + \frac{3k_F}{8\pi^2(1 + m_\pi/m_N)}\tilde{b}_0^2\right)\rho, \quad (21)$$

$$\chi_s^{02} = \left(\tilde{b}_0 + \frac{3k_F}{4\pi^2(1 + m_\pi/m_N)}\left(\tilde{b}_0^2 - \tilde{b}_1^2\right)\right)\rho, \quad (22)$$

$$\chi_p^0 = \frac{2\pi c^+}{1 + 4\pi g' c^+} + \frac{2\pi c^-}{1 + 4\pi g' c^-} \quad (23)$$

with

$$c^\pm \equiv \frac{c_0\rho \mp c_1\delta\rho}{1 + m_\pi/m_N}, \quad (24)$$

$$\Delta\chi_s = \tilde{b}_1\delta\rho, \quad \Delta\chi_p = -\frac{2\pi m_\pi}{m_\pi + m_N}\,c_1\left(\nabla^2\delta\rho\right). \quad (25)$$

Note the explicit occurrence of gradient density terms in the last expression which especially operate at the surface of finite nuclei and vanish in homogenous nuclear matter; compare Ref. [44] with [43].

3.3 Quantization of the in-medium Skyrme model

By essentially copying the steps of Sect. 2.2, one can find the following expression for the spatially integrated medium-dependent Lagrangian (20), see Refs. [43,44] for more details:

$$\begin{aligned}\int \mathrm{d}^3r\,\mathcal{L}^* = &-M^*_{\rm NP} - \mathcal{M}^2_{\Delta}\Lambda_{\rm mes} + \frac{\omega_1^2+\omega_2^2}{2}\Lambda^*_{\omega\omega,12} \\ &- (\omega_1\Omega_1+\omega_2\Omega_2)\Lambda^*_{\omega\Omega,12} + \frac{\Omega_1^2+\Omega_2^2}{2}\Lambda^*_{\Omega\Omega,12} \\ &+ \frac{(\omega_3-\Omega_3+a^*)^2}{2}\Lambda^*_{\omega\Omega,33} + (\omega_3-\Omega_3+a^*)\Lambda^*_{\rm env}\,.\end{aligned}$$

Here ω_i and Ω_i are the angular velocities in isotopic and coordinate space, respectively, while $\Lambda^*_{\omega\omega,ij}$, $\Lambda^*_{\omega\Omega,ij}$ and $\Lambda^*_{\Omega\Omega,ij}$ are the pertinent medium-dependent moments-of-inertia. Finally, $\Lambda^*_{\rm env}$ is the medium-dependent coefficient of the angular velocity sum $(\omega_3-\Omega_3+a^*)$ generated by the environment-induced isospin breaking term $\Delta\mathcal{L}^*_{\rm env}$.

Constructing the pertinent Hamiltonian by standard means and sandwiching it between the usual isospin-spin states, one can determined the energy of a nucleon (or delta) state classified by the total isospin T and third component T_3 as

$$\begin{aligned}E = &\,M^*_{\rm NP} + \mathcal{M}^2_{\Delta}\Lambda_{\rm mes} + \frac{\Lambda^{*2}_{\rm env}}{2\Lambda^*_{\omega\Omega,33}} \\ &+ \frac{\Lambda^*_{\Omega\Omega,12}+\Lambda^*_{\omega\omega,12}-2\Lambda^*_{\omega\Omega,12}}{2(\Lambda^*_{\omega\omega,12}\Lambda^*_{\Omega\Omega,12}-\Lambda^{*2}_{\omega\Omega,12})}\Big(T(T+1)-T_3^2\Big) \\ &+ \frac{T_3^2}{2\Lambda^*_{\omega\Omega,33}} - \left(a_c^* + \frac{\Lambda^*_{\rm env}}{\Lambda^*_{\omega\Omega,33}}\right)T_3\,. \qquad (26)\end{aligned}$$

Consequently, the strong part of the neutron-proton mass difference in the interior of a nucleus can be isolated from the last term of Eq. (26) and takes the form

$$\Delta m^{*(\rm strong)}_{\rm np} = a_c^* + \frac{\Lambda^*_{\rm env}}{\Lambda^*_{\omega\Omega,33}} \qquad (27)$$

with $a_c^* = \sqrt{2\mathcal{M}^2_{\Delta}\Lambda_{\rm mes}/\Lambda^*_{\omega\Omega,33}}$.

4 Skyrmion at the center of a nucleus

The knowledge of Eqs. (26) and (27) allows to construct the total mass of a proton (neutron) and the strong contribution to neutron-proton mass difference when the nucleon is located at the core of a nucleus.

In order to determined the total in-medium neutron-proton mass splitting, the electric (E) and magnetic (M) form factors of the nucleons must be utilized in addition:

$$\begin{aligned}G^*_{\rm E}(\mathbf{q}^2) &= \tfrac{1}{2}\int \mathrm{d}^3r\, e^{i\mathbf{q}\cdot\mathbf{r}}\, j^0(\mathbf{r})\,, \\ G^*_{\rm M}(\mathbf{q}^2) &= \frac{m_N}{2}\int \mathrm{d}^3r\, e^{i\mathbf{q}\cdot\mathbf{r}}[\mathbf{r}\times\mathbf{j}(\mathbf{r})]\,,\end{aligned}$$

where $\mathbf{q}$ is the transferred momentum. Furthermore, j^0 and $\mathbf{j}$ correspond to the time and space components of the properly normalized sum of the density-dependent baryonic current B^*_μ and the third component of the isovector current $\mathbf{V}^*_\mu$ of the Skyrme model; for more details see Refs. [43,44].

The electromagnetic part of the neutron-proton mass difference is then calculated in terms of the scalar (S) and isovector (V) electric (E) and magnetic (M) form factors according to the formula

$$\begin{aligned}\Delta m^{*(\rm EM)}_{\rm np} = -\frac{4\alpha}{\pi}\int_0^\infty \mathrm{d}q\Big\{&G^{\rm S*}_{\rm E}(\mathbf{q}^2)G^{\rm V*}_{\rm E}(\mathbf{q}^2) \\ &- \frac{\mathbf{q}^2}{2m_N^2}G^{\rm S*}_{\rm M}(\mathbf{q}^2)G^{\rm V*}_{\rm M}(\mathbf{q}^2)\Big\} \qquad (28)\end{aligned}$$

of Ref. [45], where α is the electric fine structure constant.

Explicit expressions of the pertinent scalar and isovector charge densities ($\rho^{\rm S,V}_{\rm E}$) and magnetic densities ($\rho^{S,V}_{\rm M}$) can be found in Ref. [44]. The rms radii $\langle r^2\rangle^{*1/2}_{\rm E,S}$ and $\langle r^2\rangle^{*1/2}_{\rm E,V}$ are calculated from the charge densities in the standard way, whereas the in-medium magnetic moments of the proton and neutron follow from calculating the sum and difference of the integrated scalar and isovector magnetic densities, respectively. Explicit expressions for the in-medium skyrmion mass $M^*_{\rm NP}$ and the moments-of-inertia appearing in Eqs. (26) and (27) can be found in Refs. [44] as well.

In summary, the (in-medium) mass of the proton, the total and electromagnetic contribution of the (in-medium) neutron-proton mass splitting, the (in-medium) magnetic moments of the proton and neutron and the isocalar and isovector (in-medium) rms radii are listed in Table 1 for the following situation: either a skyrmion in free space or located at the center of a finite nucleus core (*e.g.* ^{14}N, ^{16}O, ^{38}N, ^{40}Ca) is quantized as a proton (or neutron). In the case that it is quantized as a proton, the resulting total nuclei will be ^{15}O , ^{17}F, ^{39}Ca, ^{41}Sc, respectively; in the case of a neutron, the resulting nuclei are ^{15}N, ^{17}O, ^{39}N, ^{41}Ca instead.

In accordance with previous calculations for infinite nuclear matter in the isospin-symmetric case [42], the second and third columns of Table 1 show that the total and electromagnetic part, respectively, of the neutron-proton mass difference are slightly increased in finite nuclei relative to the vacuum case. Furthermore, the present model predicts (see the first column of Table 1) that the effective nucleon mass is strongly reduced at the center of the nucleus. We will return to this point later on when we discuss the Nolen-Schiffer anomaly in Sect. 8.

Finally, the increase in the tabulated in-medium values of the magnetic moments and rms charge radii is compatible with the hypothesis of the nucleon-swelling in a nuclear background which was already confirmed by the isospin-symmetric calculations of Refs. [38–40] for the medium-modified Skyrme model; see also the static in-medium results of Refs. [42,43].

Table 1. Static properties of a nucleon when the pertinent skyrmion is either in free space of added to the center of a finite nucleus core, namely ^{14}N, ^{16}O, ^{38}K, and ^{40}Ca, respectively, such that a proton or the total nucleus ^{15}O, ^{17}F, ^{39}Ca, and ^{41}Sc results. Here $m_{\rm p}^*$ is the in-medium proton mass, $\Delta m_{\rm np}^*$ is the in-medium neutron-proton mass difference and $\Delta m_{\rm np}^{*({\rm EM})}$ is its electromagnetic part. Furthermore, $\mu_{\rm p}^*$ and $\mu_{\rm n}^*$ are the in-medium proton and neutron magnetic moments in units of the free-space Bohr magnetons (n.m.). Finally, $\langle r^2\rangle_{\rm E,S}^{*1/2}$ and $\langle r^2\rangle_{\rm E,V}^{*1/2}$ are the in-medium isoscalar (S) and isovector (V) charge radii of the nucleon inside a nucleus. For more details see Ref. [44].

Core → Elem.	$m_{\rm p}^*$ [MeV]	$\Delta m_{\rm np}^*$ [MeV]	$\Delta m_{\rm np}^{*({\rm EM})}$ [MeV]	$\mu_{\rm p}^*$ [n.m.]	$\mu_{\rm n}^*$ [n.m.]	$\langle r^2\rangle_{\rm E,S}^{*1/2}$ [fm]	$\langle r^2\rangle_{\rm E,V}^{*1/2}$ [fm]
Vac.→ p	938.268	1.291	-0.686	1.963	-1.236	0.481	0.739
^{14}N → ^{15}O	593.285	1.668	-0.526	2.355	-1.276	0.656	0.850
^{16}O → ^{17}F	585.487	1.697	-0.517	2.393	-1.297	0.667	0.863
^{38}K → ^{39}Ca	558.088	1.804	-0.480	2.584	-1.422	0.722	0.942
^{40}Ca→^{41}Sc	557.621	1.804	-0.478	2.569	-1.428	0.724	0.947

5 Skyrmion off-centered in a nucleus

Whereas the results of the last section hold for the case that the skyrmion is at the center of a symmetrical core of a nucleus, the results of this section apply for the more general situation that the skyrmion is located at a distance R from the center of a finite nucleus, as specified in Fig. 1. Note that in this case the spherical symmetric hedgehog ansatz cannot be used anymore, since the background – as viewed from the center of the *skyrmion* – is not spherically symmetric. Thus there exists further deformations in the isotopic and in the coordinate space [38, 39]. In this case a variational ansatz can still be used which allows for more freedom in the radial and especially in the angular coordinates than the hedgehog form would do, but is still compatible with the quantization procedure. See Ref. [44] for more details on this variational parameterization. In this reference, it was also checked that the results of the variational computation merge with the ones of the hedgehog computation when the skyrmion is moved back to the center of the nucleus.

Fig. 1. A sketch of a skyrmion located inside a finite nucleus with $R = |\mathbf{R}|$ the separation between the geometrical center (O') of the skyrmion and the center (O) of the nucleus. The vectors (angles) $\mathbf{r}$ (θ) and $\mathbf{r}'$ (θ') refer to the body-fixed coordinates of the nucleus and skyrmion, respectively. Since the nucleus is spherically symmetric, both coordinate systems can be orientated in such a way that their z-axes coincide.

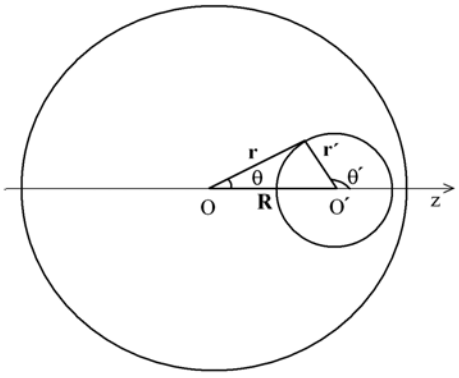

5.1 Effective proton mass m_p^* inside a nucleus

First, we will show in Fig. 2 the results of Ref. [44] for the effective proton mass $m_{\rm p}^*$ as function of the distances between the geometrical center of the pertinent skyrmion and the center of the core-nucleus, *i.e.* ^{14}N, ^{16}O, ^{38}K, and ^{40}Ca. When the skyrmion is quantized as a proton, the resulting nuclei are ^{15}O, ^{17}F, ^{39}Ca, and ^{41}Sc, respectively. Note that the in-medium mass of the proton $m_{\rm p}^*$ starts with the value listed in Table 1 when its is near the center of the nucleus – in agreement with the statements at the end of the last section. With increasing distance from the center of the nucleus the value of the effective mass monotonically increases, until it smoothly approaches the free space value $m_{\rm p}$ at the border of the nucleus.

We will come back to the effective nucleon mass when we discuss the Nolen-Schiffer anomaly in Sect. 8. In the following we will concentrate on the effective in-medium neutron-proton mass *difference*.

5.2 Effective neutron-proton mass difference

In Fig. 3 the behavior of the strong part of the in-medium neutron-proton mass difference can be found for the same notations and input as in Fig. 2.

Note that the strong part of the in-medium mass difference has a non-monotonic behavior. This follows from the fact that the density is a local quantity and that additional isospin-breaking contributions arise due to the density gradients resulting from the p-wave pion-nucleus scattering, see Eq. (25). Especially, it can be observed that in the surface region of each nucleus, where the density gradients are large and the local isospin asymmetry in the nuclear background is high, the value of $\Delta m_{\rm np}^{*({\rm strong})}$ is at an extremum.

Fig. 2. The dependence of the effective mass of the proton m_p^* on the distance R between the center of the skyrmion and the center of the nucleus. The solid curve represents the case that a skyrmion – quantized as a proton – is added to a ^{14}N nucleus, giving ^{15}O in total. The dot-dashed curve refers to the case of a ^{16}O nucleus $\rightarrow$ ^{17}F in total. The dashed curve stands for the case of ^{38}K $\rightarrow$ ^{39}Ca and the dotted curve represents the case of ^{40}Ca $\rightarrow$ ^{41}Sc. The horizontal line marks the free space value of the proton mass. Figure from Ref. [44].

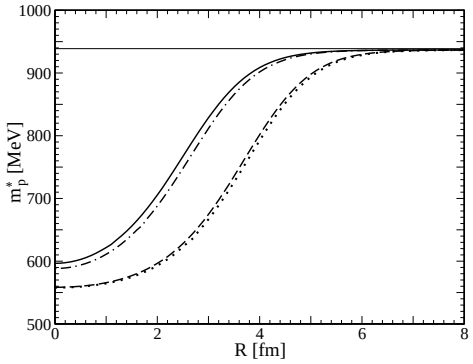

Fig. 3. The dependence of $\Delta m_{np}^{*(strong)}$ on the distance R between the center of the skyrmion and the center of the nucleus. The notations and input are the same as in Fig. 2, with the exception that the horizontal line marks the free space value $\Delta m_{np}^{(strong)} = 2.0$ MeV. Figure from Ref. [44].

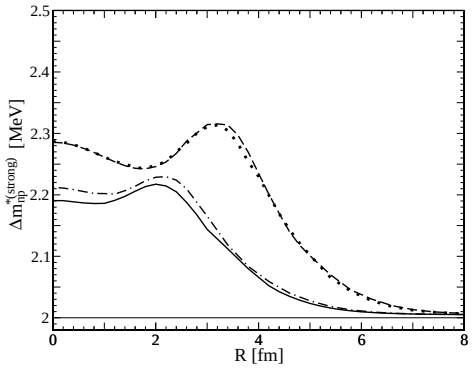

In Fig. 4 the electromagnetic part of the in-medium neutron-proton mass difference is shown for the same nuclei as before. It can be seen that the variations in the electromagnetic part of the effective neutron-proton mass differences are small as compared with their strong counter parts. Furthermore, $\Delta m_{np}^{*(EM)}$ nearly monotonically decreases with increasing distance from the center. Note that the values at $R = 0$ agree of course with the values listed in Table 1.

Finally, for completeness, in Fig. 5 the dependence of the total effective neutron-proton mass difference Δm_{np}^* on the distance R is shown for the same nuclei as specified above. Again, the values at $R = 0$ agree with the values listed in Table 1.

Fig. 4. The dependence of $\Delta m_{np}^{*(EM)}$ on the distance R between the center of the skyrmion and the center of the nucleus. The notations and input are the same as in Fig. 2, with the exception that the horizontal line marks the free space value $\Delta m_{np}^{(EM)} = -0.69$ MeV. Figure from Ref. [44].

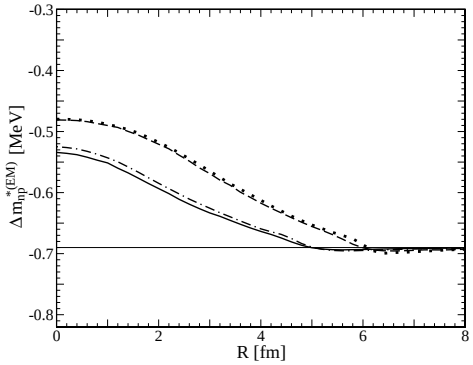

Fig. 5. The dependence of the total in-medium neutron-proton mass difference Δm_{np}^* on the distance R between the center of the skyrmion and the center of the nucleus. The notations and input are the same as in Fig. 2, with the exception that the horizontal line marks the free space value $\Delta m_{np} = 1.3$ MeV. Figure from Ref. [44].

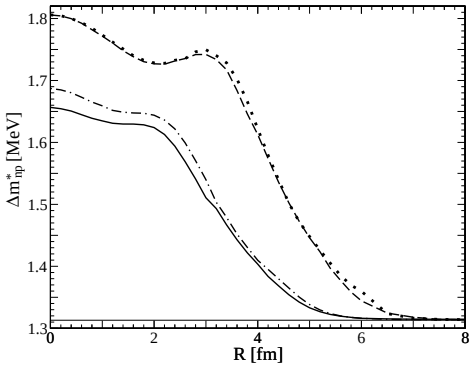

6 Neutron-proton mass difference in nuclear matter

The densities of the finite nuclei discussed here and in Ref. [44] correspond closely to the isosymmetric nuclear matter case studied in Refs. [42,43], where a moderate increase of the effective neutron-proton difference, compatible with Fig. 3 or Fig. 5, can be observed. In neutron matter, however, as Ref. [43] shows, there is a pronounced decrease of the in-medium neutron-proton mass difference with increasing density.

Therefore, instead of discussing the density-variations of all the static quantities in an infinite nuclear matter background as in Ref. [43], we report here only about the effective neutron-proton mass differences in nuclear matter studied in Ref. [43].

In Fig. 6 the strong part of the in-medium neutron-proton mass splitting in nuclear matter, Δm_{np}^*, is shown for isospin-symmetric nuclear matter (solid curve), neutron-

rich matter (dashed curve), pure neutron matter (dotted curve), and proton-rich matter (dot-dashed curve). Especially, when the isospin symmetry of nuclear matter is broken, $\Delta m_{\rm np}^{*(\rm strong)}$ strongly varies (see the dashed and dot-dashed curves in Fig. 6). In pure neutron matter the change becomes very drastic (see the dotted curve in Fig. 6), and $\Delta m_{\rm np}^{*(\rm strong)}$ decreases very rapidly with increasing density.

Fig. 6. Density dependence of the strong part $\Delta m_{\rm np}^{*(\rm strong)}$ of the neutron-proton mass difference in nuclear matter. The abscissa represents the density ρ normalized to the saturation density of ordinary nuclear matter $\rho_0 = 0.5 m_\pi^3$, while the ordinate shows the mass difference in units of MeV. The result in isospin-symmetric matter is plotted as a solid curve, the result of neutron-rich matter with $\delta\rho/\rho = 0.2$ as dashed curve, the dotted curve represents pure neutron matter ($\delta\rho/\rho = 1$) and the dot-dashed curve proton-rich matter with $\delta\rho/\rho = -0.2$. Figure from Ref. [43].

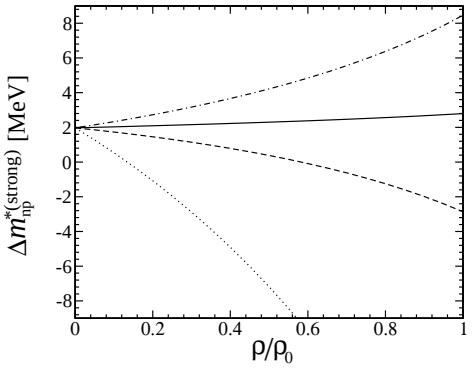

In contrast to the strong part, the electromagnetic part of the neutron-proton mass difference in nuclear matter varies only by a very small amount when the isospin-asymmetry parameter $\delta\rho/\rho$ is increased (see Fig. 7).

Fig. 7. Density dependence of the electromagnetic part $\Delta m_{\rm np}^{*(\rm EM)}$ of the neutron-proton mass difference in nuclear matter. The axes and curves are defined as in Fig. 6. Figure from Ref. [43].

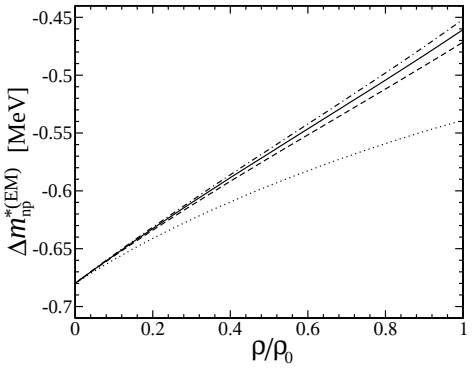

Again, for completeness, the total neutron-proton mass difference in nuclear matter is presented in Fig. 8. The difference to the purely strong case, shown in Fig. 6, is hardly visible.

Fig. 8. Density dependence of the total neutron-proton mass difference $\Delta m_{\rm np}^{*}$ in nuclear matter. The axes and curves are defined as in Fig. 6. Figure from Ref. [43].

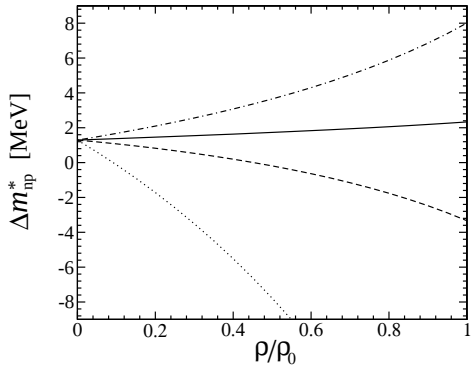

7 Tentative Conclusions

In summary, we have studied the effective neutron-proton mass difference $\Delta m_{\rm np}^{*}$ in finite nuclei in the framework of an isospin- and medium-modified Skyrme model.

The in-medium mass of the proton starts near the center of the nucleus with a strongly reduced value and increases monotonically with increasing distance from the center. The strong part of the effective neutron-proton mass difference has a non-monotonic behavior because of the additional isospin-breaking contributions due to the gradients arising from the *p*-wave pion-nucleus scattering. There is an extremum of $\Delta_{\rm np}^{*\,\rm strong}$ at the surface of the nucleus because there the gradients are large and the isospin asymmetry in the nuclear background is high. The electromagnetic part of the effective neutron-proton mass difference is negative and increases monotonically in magnitude with increasing distance from the center. In magnitude its value is small as compared with its strong counter part. The other static quantities (in-medium magnetic moments, rms charge radii etc.) behave according to the nucleon-swelling hypothesis for a nucleon embedded in the medium.

While in isosymmetric backgrounds the effective neutron-proton mass difference moderately increases, in asymmetric nuclear matter the strong part of this quantity can vary markedly (upwards in proton-rich matter and downwards in neutron-rich matter), whereas the electromagnetic contribution is always small and subleading. Especially in neutron matter, there is a strong decrease of the (strong and also the total) neutron-proton mass difference with increasing density.

8 Nolen-Schiffer anomaly

A long standing problem in nuclear physics is the Nolen-Schiffer anomaly observed in mirror nuclei [18,19]. Here

we will show how the Nolen-Schiffer anomaly can be treated in the framework of an isospin- and medium modified generalized Skyrme model.

The mass difference between mirror nuclei

$$\Delta M \equiv {}^{A}_{Z+1}M_N - {}^{A}_{Z}M_{N+1} \tag{29}$$

which differ by one unit in their charges, $\Delta Z = 1$, can very precisely be measured and is usually split into two terms

$$\Delta M = \Delta E_{\rm EM} - \Delta m_{\rm np} - \left(\Delta m^*_{\rm np} - \Delta m_{\rm np}\right). \tag{30}$$

The first contribution is the Coulomb energy difference $\Delta E_{\rm EM}$ computed relatively to the free neutron-proton mass difference, whereas the second is the in-medium neutron-proton mass difference subtracted from the free one and therefore the net in-medium change of this quantity. The Coulomb energy difference includes various corrections, *e.g.*, by exchange terms, the center-of-mass motion, finite size effects of the proton and neutron distributions, magnetic interactions, vacuum effects, short-range two-body correlations etc. It can be calculated with great accuracy (within 1 % error) [19]. If $\Delta m^*_{\rm np}$ is assumed to be constant and equal to the vacuum value, then Eq. (30) cannot be satisfied. This phenomenon is called the Nolen-Schiffer-anomaly (NSA). Quantitatively, the NSA ranges – throughout the periodic table – from a few hundred keV for the lightest nuclei up to several MeV for the heaviest ones. A possible resolution is the assumption that the effective neutron-proton mass difference would decrease with increasing mass number A, such that

$$\Delta_{NSA} = \Delta m_{\rm np} - \Delta m^*_{\rm np}\,. \tag{31}$$

Within the present approach $\Delta m^*_{\rm np}$ has a local R dependence according to the location of the nucleons inside the nuclei as shown in Fig. 5. In order to compare these results with the experimental data one therefore has to average the value of $\Delta m^*_{\rm np}$ with respect to the separation R. Since the nucleons inducing the Nolen-Schiffer anomaly are valence nucleons, these must be located in the peripheral region of each of the mirror nuclei, if the latter differ by one particle or hole from a (magic) closed-shell nucleus. The averaged effective masses and splittings can therefore be expressed as follows:

$$\begin{aligned}
\overline{m}^*_{\rm n} &\equiv \int m^*_{\rm n}(R)\left|\psi_{\rm n}(R)\right|^2 {\rm d}^3R\,,\\
\overline{m}^*_{\rm p} &\equiv \int m^*_{\rm p}(R)\left|\psi_{\rm p}(R)\right|^2 {\rm d}^3R\,,\\
\Delta\overline{m}^*_{\rm np} &\equiv \overline{m}^*_{\rm n} - \overline{m}^*_{\rm p}\,,
\end{aligned} \tag{32}$$

where $|\psi_{\rm n}(R)|^2$ and $|\psi_{\rm p}(R)|^2$ are the density distributions of the in-medium neutron and proton, respectively. In terms of the difference of the density distributions

$$\Delta\psi^2_{\rm np}(R) \equiv \left|\psi_{\rm n}(R)\right|^2 - \left|\psi_{\rm p}(R)\right|^2,$$

Eq. (32) can be rewritten as

$$\begin{aligned}
\Delta\overline{m}^*_{\rm np} &\approx \int\left\{\Delta\psi^2_{\rm np}(R)\, m^*_{\rm p}(R) + \Delta m^*_{\rm np}(R)\,|\psi_{\rm p}(R)|^2\right\}{\rm d}^3R\\
&\equiv \Delta\overline{m}^{*(1)}_{\rm np} + \Delta\overline{m}^{*(2)}_{\rm np}\,,
\end{aligned} \tag{33}$$

where the subleading contribution of the cross term

$$\int \Delta\psi^2_{\rm np}\,\Delta m^*_{\rm np}\,{\rm d}^3R$$

is neglected. Thus here the Nolen-Schiffer anomaly simply reads

$$\overline{\Delta}_{\rm NSA} = \Delta m_{\rm np} - \left(\Delta m^{*(1)}_{\rm np} + \Delta m^{*(2)}_{\rm np}\right). \tag{34}$$

It is listed in Table 2, left panel (labeled 'α=0') of the third column (labeled 'Present approach') for chosen pairs of mirror nuclei, such that the overall mass number A increases.

Whereas qualitatively the calculated NSA values have the correct A behavior, quantitatively the results are more than one order of magnitude too big (compare with the empirical values listed in the last column of Table 2). This can be traced back to the pronounced negative shift of $\Delta\overline{m}^{*(1)}_{\rm np}$ (see the first entry of the third column of Table 2). This shift is mainly there for three reasons:

(i) the rather large renormalization of the effective nucleon mass,
(ii) the pronounced R dependence of $m^*_{\rm p}$ inside the nucleus (see Fig. 2), and
(iii) the relative swelling of the proton distributions due to the Coulomb factor, *i.e.* $\Delta\psi^2_{\rm np} \neq 0$.

For example, the averaged in-medium mass of the valence proton in ^{17}O is reduced to $\overline{m}^*_{\rm p} = 812.35$ MeV. This drop of about 125 MeV is very large in comparison with the empirical value of the binding energy per nucleon in nuclear matter. For heavier nuclei, where the density in the interior approximates the normal nuclear matter density, the drop of the averaged effective mass is even larger, *e.g.* $m_{\rm p} - \overline{m}^*_{\rm p} \sim (150 - 200)$ MeV in the ^{40}Ca region (see the second column of Table 2) down to ~ 300 MeV in the ^{208}Pb region.

If solely the contribution $\Delta\overline{m}^{*(2)}_{\rm np}$ (due to the explicit R dependence of the neutron-proton mass difference) were considered, then the NSA in the present approach would even have a negative sign: $\Delta m_{\rm np} - \Delta\overline{m}^{*(2)}_{\rm np} < 0$.

Instead of driving the input parameters of Sect. 3.1 to unphysical values in order to match the NSA discrepancy, we suggested in Ref. [44] to invert the problem and to estimate the effective nucleon mass inside finite nuclei according to the results in the isospin-breaking sector. To perform this task an artificially added renormalization parameter $\alpha_{\rm ren}$ in the expression

$$m^*_{\rm n,p}(R,\alpha_{\rm ren}) = m^*_{\rm n,p}(R) + \left(m_{\rm n,p} - m^*_{\rm n,p}(R)\right)\alpha_{\rm ren} \tag{35}$$

of the effective nucleon mass is fine-tuned in such a way, that the Nolen-Schiffer anomaly is satisfied. The results are presented in Table 2, fourth column labeled '$\alpha_{\rm ren} = 0.95$'. It can be seen that a successful description of the correct order of the NSA implies a rather small drop of the mass of the valence nucleons: $m_{\rm n,p} - \overline{m}^*_{\rm n,p}(\alpha_{\rm ren} = 0.95) \sim 10$ MeV which is close to the empirical binding energy per nucleon in nuclear matter. In this case, the contribution to the Nolen-Schiffer anomaly from the term $\Delta\overline{m}^{*(2)}_{\rm np}$ can be neglected: $\Delta m_{\rm np} - \Delta\overline{m}^{*(2)}_{\rm np}(\alpha_{\rm ren} = 0.95) \sim -0.02$ MeV.

Table 2. The averaged mass $\overline{m}^*_p$ of the valence proton in a given nucleus, the contributions to the effective neutron-proton mass difference (see Eq. (33)) and the Nolen-Schiffer discrepancy $\overline{\Delta}_{NSA}$ calculated in the present approach by Eq. (34) or Eq. (35) and the corresponding "empirical" results of Ref. [19]. All quantities are in units of MeV.

Nuclei	$\overline{m}^*_p$		Present approach						$\overline{\Delta}^{empirical}_{NSA}$
			$\alpha_{ren} = 0$			$\alpha_{ren} = 0.95$			
	$\alpha_{ren}=0$	$\alpha_{ren}=0.95$	$\Delta\overline{m}^{*(1)}_{np}$	$\Delta\overline{m}^{*(2)}_{np}$	$\overline{\Delta}_{NSA}$	$\Delta\overline{m}^{*(1)}_{np}$	$\Delta\overline{m}^{*(2)}_{np}$	$\overline{\Delta}_{NSA}$	Ref. [19]
^{15}O-^{15}N	767.45	928.30	-4.27	1.56	4.02	-0.21	1.33	0.20	0.16 ± 0.04
^{17}F-^{17}O	812.35	930.54	-5.53	1.52	5.33	-0.28	1.32	0.27	0.31 ± 0.04
^{39}Ca-^{39}K	724.78	926.16	-8.11	1.67	7.75	-0.41	1.33	0.37	0.22 ± 0.08
^{41}Sc-^{41}Ca	771.71	928.51	-9.74	1.62	9.44	-0.49	1.33	0.47	0.59 ± 0.08

9 Final remarks

Let us discuss the relevance of our results for the Nolen-Schiffer anomaly. Qualitatively, our approach predicts the sign and the relative mass-number increase of this anomaly. But quantitatively it is far from satisfactory: the results are more than one order of magnitude too large. Clearly, the part of our calculation relevant to the Nolen-Schiffer anomaly depends on the proton and neutron distributions of the mirror nuclei and is very sensitive to the behavior of the wave functions of the valence nucleons in the peripheral region of the nucleus. We have pointed out the possibility that the Nolen-Schiffer anomaly may rather follow from the behavior of the effective nucleon mass in finite nuclei than from the effective neutron-proton mass difference: our calculations imply that the Nolen-Schiffer anomaly could not and, maybe, should not be saturated by $\Delta\overline{m}^{*(2)}_{np}$ (the averaged contribution due to the explicit density and radial dependence of the neutron-proton mass difference). Rather more important is $\Delta\overline{m}^{*(1)}_{np}$, the contribution due to the difference in the squared wave functions of valence proton and neutron weighted by the local (density and density-gradient induced) variation of the effective mass of the nucleon. In fact, when we restrict the in-medium reduction of the (averaged effective) proton mass to about 1 % of the free proton mass – a value which is compatible with the empirical binding energy per nucleon in nuclear matter – we obtain a rather precise description of the NSA. Here, we should remark that the gradient terms which are present in our model do not noticeably affect the scaling behavior of m^*. They are important for the surface behavior of Δm^*_{np}, though.

The calculated Coulomb energy differences ΔE_{EM} (30) for mirror nuclei of Ref. [19] incorporate a contribution due to the different wave functions of valence nucleons that is known as Thomas-Ehrman effect [46,47]. Note, however, that in Ref. [19] a constant, *R*-independent value of the nucleon mass – namely the free mass in vacuum – was used, whereas here the effect is based on the *R-dependence* of the effective nucleon mass.

In summary, the possibility exists that the anomaly of the mirror nuclei can be saturated by invoking a dynamical (local) mass of the nucleon that needs to be only slightly reduced in comparison to its free counter part. In this context, it should be pointed out that the anomaly could also be removed by the introduction of an additional term into the Coulomb part of the energy density of nuclear systems in the local-density-functional approach [48–51]. In fact, this term is chosen such that it is proportional to the *isoscalar* rather than to the *isovector* density. Furthermore, it should be stressed that the isoscalar contribution is surface dominated. It is even argued in Refs. [52,53] that the effective-to-free-nucleon-mass ratio m^*_N/m_N is unity to within a few percent. Apparently, different model calculations can lead to similar conclusions about the origin of the Nolen-Schiffer anomaly.

Returning to the in-medium modified Skyrme model, we would like to point out that the results might still be improved if the calculations can be made more self-consistent, *e.g.*, by the incorporation of feedback mechanisms between the modified skyrmion and the local nuclear background. In addition, the inclusion of further degrees of freedom might be a useful possibility as their introduction can anyhow be motivated by more detailed considerations about the nucleon structure and the nucleon-nucleon interaction. Also the non-local character of the effective nucleon mass may be of importance.

Acknowledgement

We would like to thank Horst Lenske for useful discussions and a computer code calculating nuclear densities of finite nuclei. We are also grateful to Frank Grümmer for providing us with calculated shell-model wave functions. The work of U.T.Y. was supported by the Alexander von Humboldt Foundation. The work of A.M.R. was supported by the second phase of the Brain Korea 21 Project in 2007 and by the German Academic Exchange Service DAAD. Partial financial support from the EU Integrated Infrastructure Initiative Hadron Physics Project (contract number RII3-CT-2004-506078), by the DFG (TR 16, "Subnuclear Structure of Matter") and by BMBF (research grant 06BN411) is gratefully acknowledged. This work is partially supported by the Helmholtz Association through funds provided to the virtual institute "Spin and strong QCD" (VH-VI-231).

References

1. B.A. Li, C.M. Ko and W. Bauer, Int. J. Mod. Phys. E **7** (1998) 147 [arXiv:nucl-th/9707014]
2. V. Baran, M. Colonna, V. Greco and M. Di Toro, Phys. Rept. **410** (2005) 335 [arXiv:nucl-th/0412060]
3. A.W. Steiner, M. Prakash, J.M. Lattimer and P.J. Ellis, Phys. Rept. **411** (2005) 325 [arXiv:nucl-th/0410066]
4. M. Lopez-Quelle, S. Marcos, R. Niembro, A. Bouyssy and V.G. Nguyen, Nucl. Phys. A **483** (1988) 479
5. I. Bombaci and U. Lombardo, Phys. Rev. C **44** (1991) 1892
6. E. Chabanat, J. Meyer, P. Bonche, R. Schaeffer and P. Haensel, Nucl. Phys. A **627** (1997) 710
7. S. Kubis and M. Kutschera, Phys. Lett. B **399** (1997) 191 [arXiv:astro-ph/9703049]
8. W. Zuo, I. Bombaci and U. Lombardo, Phys. Rev. C **60** (1999) 024605 [arXiv:nucl-th/0102035]
9. K. Tsushima, K. Saito and A. W. Thomas, Phys. Lett. B **465** (1999) 36 [arXiv:nucl-th/9907101]
10. V. Greco, M. Colonna, M. Di Toro, G. Fabbri and F. Matera, Phys. Rev. C **64** (2001) 045203 (2001)
11. F. Hofmann, C.M. Keil and H. Lenske, Phys. Rev. C **64** (2001) 034314 (2001) [arXiv:nucl-th/0007050]
12. B. Liu, V. Greco, V. Baran, M. Colonna and M. Di Toro, Phys. Rev. C **65** (2002) 045201
13. W. Zuo, L.G. Cao, B.A. Li, U. Lombardo and C.W. Shen, Phys. Rev. C **72** (2005) 014005 [arXiv:nucl-th/0506003]
14. E.N.E. van Dalen, C. Fuchs and A. Faessler, Phys. Rev. Lett. **95** (2005) 022302 [arXiv:nucl-th/0502064]
15. T. Lesinski, K. Bennaceur, T. Duguet and J. Meyer, Phys. Rev. C **74** (2006) 044315 [arXiv:nucl-th/0607065]
16. E.N.E. van Dalen, C. Fuchs and A. Faessler, Eur. Phys. J. A **31** (2007) 29 [arXiv:nucl-th/0612066]
17. L.W. Chen, C.M. Ko, B.A. Li and G.C. Yong, arXiv:0704.2340 [nucl-th]
18. J.A. Nolen and J.P. Schiffer, Ann. Rev. Nucl. Part. Sci. **19** (1969) 471
19. S. Shlomo, Rep. Prog. Phys. **41** (1978) 957
20. S. Shlomo, Physica Scr. **26** (1982) 280
21. E.M. Henley and G. Krein, Phys. Rev. Lett. **62** (1989) 2586
22. T. Hatsuda, H. Hogaasen and M. Prakash, Phys. Rev. Lett. **66** (1991) 2851 [Erratum-ibid. **69** (1992) 1290]
23. A.G. Williams and A.W. Thomas, Phys. Rev. C **33** (1986) 1070
24. T.D. Cohen, R.J. Furnstahl and M.K. Banerjee, Phys. Rev. C **43** (1991) 357
25. M.H. Shahnas, Phys. Rev. C **50** (1994) 2346
26. C.J. Horowitz, J. Piekarewicz, Phys. Rev. C **63** (2000) 011303R
27. T. Suzuki, H. Sagawa and A. Arima, Nucl. Phys. **A536** (1992) 141
28. T. Schafer, V. Koch and G.E. Brown, Nucl. Phys. A **562** (1993) 644
29. E.G. Drukarev and M.G. Ryskin, Nucl. Phys. A **572** (1994) 560
30. C. Adami and G.E. Brown, Z. Phys. A **340** (1991) 93
31. B.K. Agrawal, T. Sil, S.K. Samaddar, J.N. De and S. Shlomo, Phys. Rev. C **64** (2001) 024305
32. T.H.R. Skyrme, Proc. Roy. Soc. Lond. A **260** (1961) 127
33. T.H.R. Skyrme, Nucl. Phys. **31** (1962) 556
34. G.S. Adkins, C.R. Nappi and E. Witten, Nucl. Phys. B **228** (1983) 552
35. G.S. Adkins and C.R. Nappi, Nucl. Phys. B **233** (1984) 109
36. I. Zahed and G.E. Brown, Phys. Rep. **142** (1986) 1
37. U.-G. Meißner and I. Zahed, Adv. Nucl. Phys. **17** (1986) 143
38. U.T. Yakhshiev, M.M. Musakhanov, A.M. Rakhimov, U.-G. Meißner, and A. Wirzba, Nucl. Phys. **A700** (2002) 403
39. U.T. Yakhshiev, U.-G. Meißner and A. Wirzba, Eur. Phys. J. **A16** (2003) 569
40. U.T. Yakhshiev, U.-G. Meißner, A. Wirzba, A.M. Rakhimov, and M.M. Musakhanov, Phys. Rev. **C71** (2005) 034007
41. E. Rathske, Z. Phys. A **331** (1988) 499
42. U.-G. Meißner, A.M. Rakhimov, A. Wirzba, and U.T. Yakhshiev, Eur. Phys. J. **A31** (2007) 357
43. U.-G. Meißner, A.M. Rakhimov, A. Wirzba, and U.T. Yakhshiev, Eur. Phys. J. **A32** (2007) 299
44. U.-G. Meißner, A.M. Rakhimov, A. Wirzba, and U.T. Yakhshiev, Eur. Phys. J. **A36** (2008) 37
45. J. Gasser and H. Leutwyler, Phys. Rept. **87** (1982) 77
46. R.G. Thomas, Phys. Rev. **81** (1951) 148
47. J.B. Ehrman, Phys. Rev. **81** (1951) 412
48. A. Bulgac, V.R. Shaginyan, Nucl. Phys. A **601** (1996) 103
49. S.A. Fayans, JETP Lett. **68** (1998) 169
50. A. Bulgac, V.R. Shaginyan, Eur. Phys. J. A **5** (1999) 247
51. S.A. Fayans and D. Zawischa, Int. J. Mod. Phys. B **15** (2001) 1684
52. B.A. Brown, Phys. Rev. C **58** (1998) 220
53. B.A. Brown, RIKEN Rev. **26** (2000) 53